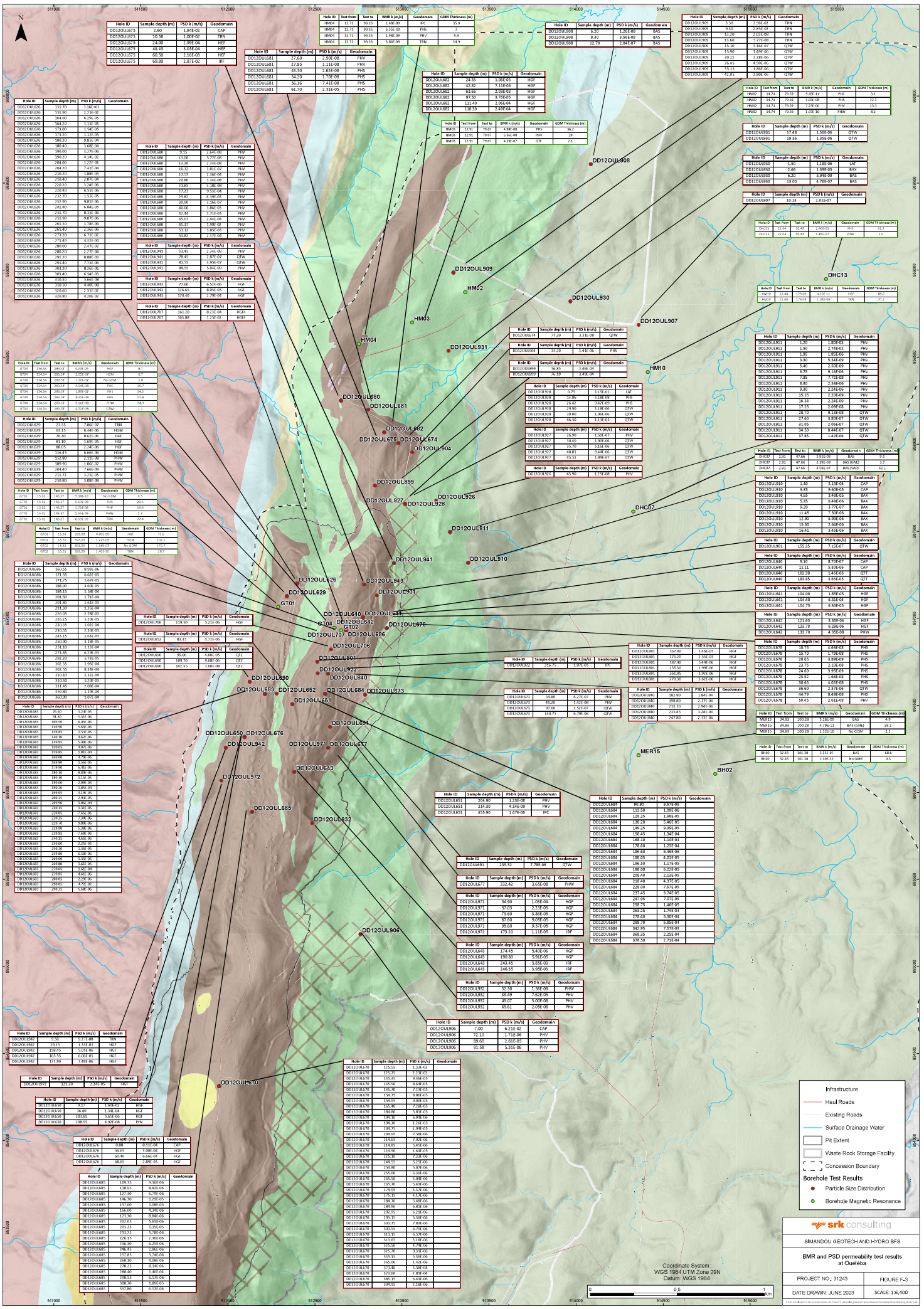
Infrastructure
Haul Roads
Existing Roads
Surface Drainage Water
Pit Extent
Waste Rock Storage Facility
Concession Boundary
Borehole Test Results
Particle Size Distribution
Borehole Magnetic Resonance
srk consulting
SIMANDOU GEOTECH AND HYDRO BFS
BMR and PSD permeability test results at Ouéléba
PROJECT NO:: 31243
FIGURE F-3
DATE DRAWN: JUNE 2023
SCALE: 1:6,400
Coordinate System: WGS 1984 UTM Zone 29N
Datum: WGS 1984
DD12OUL908
DD12OUL909
HM02
DD12OUL930
DD12OUL907
HM03
HM04
DD12OUL931
HM10
DD12OUL680
DD12OUL681
DD12OUL682
DD12OUL675
DD12OUL674
DD12OUL904
DD12OUL899
DD12OUL927
DD12OUL928
DD12OUL926
DHC07
DD12OUL911
DD12OUL941
DD12OUL910
DD12OUL626
DD12OUL943
DD12OUL629
DD12OUL901
GT01
DD12OUL640
DD12OUL633
GT04
DD12OUL642
GT02
DD12OUL678
DD12OUL707
DD12OUL686
DD12OUL706
DD12OUL803
DD12OUL922
DD12OUL840
DD12OUL690
DD12OUL683
DD12OUL652
DD12OUL684
DD12OUL673
DD12OUL651
DD12OUL694
DD12OUL650
DD12OUL676
DD12OUL942
DD12OUL971
DD12OUL677
DD12OUL643
DD12OUL972
DD12OUL685
DD12OUL932
DD12OUL906
DD12OUL670
DHC13
MER15
BH02

Laboratory Analysis on Core Permeability

Table F 1: Summary of laboratory analysis of competent core samples

Lithology	Number of samples	Porosity	Permeability
		(%)	(m/s)
Itabirite (ITA)	5	1.6 – 11.9	1.15×10^{-07} – 9.66×10^{-10}
Siliceous haematite (HS)	5	17.9 – 26.8	6.14×10^{-07} – 6.23×10^{-08}
Hard ore (M2H)	5	9.6 – 25.0	7.40×10^{-07} – 3.79×10^{-08}
Friable ore (M2F)	4	32.8 – 42.7	2.32×10^{-02} – 1.81×10^{-03}
Martite goethite hard (MGH)	5	19.9 – 33.0	2.67×10^{-07} – 3.75×10^{-10}
Weathered surface (WEA)	5	19.5 – 25.4	2.13×10^{-06} – 1.60×10^{-09}
Phyllite (PHY)	5	0.6 – 18.3	1.35×10^{-10} – 7.53×10^{-11}

Table F 2: Summary of laboratory core permeability analysis

Geodomain	No. of core samples	No. of analyses	Hydraulic conductivity (m/sec)		
			Min	Ave.	Max.
CAP	1	1	-	-	3.75×10^{-10}
HEC	8	8	1.26×10^{-08}	3.47×10^{-07}	1.34×10^{-06}
HEF	3	9	2.06×10^{-03}	9.19×10^{-03}	2.32×10^{-02}
HGC	4	4	2.30×10^{-10}	6.04×10^{-07}	2.10×10^{-06}
IPC	5	5	9.66×10^{-10}	2.85×10^{-08}	1.15×10^{-07}
IRC	2	3	1.76×10^{-07}	3.60×10^{-07}	6.92×10^{-07}
IRF	1	3	1.81×10^{-03}	1.98×10^{-03}	2.13×10^{-03}
PHC	9	12	2.41×10^{-11}	2.91×10^{-09}	1.96×10^{-08}
PHS	13	41	1.02×10^{-09}	9.46×10^{-08}	3.90×0^{-07}
PHV	5	5	1.04×10^{-10}	1.37×10^{-07}	3.46×10^{-07}
PHW	17	53	1.64×10^{-10}	5.05×10^{-08}	5.21×10^{-07}
QTW	1	2	3.48×10^{-08}	2.52×10^{-07}	4.70×10^{-07}
WEA	5	5	1.60×10^{-09}	7.36×10^{-07}	2.13×10^{-06}

Estimates of Hydraulic Conductivity by Falling Head Test

Table F 3: Falling head tests undertaken in OUL – 2008 (from SWS, 2012)

Hole ID	Dominant lithology[28]	Preliminary estimates hydraulic conductivity (m/s)
RC08OUL308	HGF	1.66×10^{-6}
RC08OUL316	PHY	9.86×10^{-9}
RC08OUL318	HGF-IRC	3.37×10^{-7}
RC08OUL323	HGF	4.54×10^{-7}
RC08OUL330	HGF	6.85×10^{-7}
RC08OUL347	HGF	1.30×10^{-7}
RC08OUL363	PHY	2.7×10^{-7}
RC08OUL382	HGF	3.0×10^{-7}
RC08OUL468	HGF	1.55×10^{-6}
DD06OUL025	HGF-PHY	5.54×10^{-8}
RD08OUL394	HGF	2.15×10^{-8}
RC07OUL066	HGF	7.47×10^{-8}
RC07OUL139	HGF	2.72×10^{-8}
DD08OUL464	HEF-PHY	7.14×10^{-10}
DD08OUL463	HGF	7.62×10^{-7}
DD08OUL462	HGF-IPC	8.37×10^{-9}
RC08OUL415	CAP-PHY	5.86×10^{-7}

[28]Le géodomaine PHY utilisé dans l'étude de 2012 a depuis été subdivisé pour tenir compte du degré d'altération (voir la 4.2). Dans ce tableau, PHY peut désigner PHS à PHC.

Table F 4: Falling head tests undertaken in OUL – 2011 to 2012 (from SWS, 2012)

BH ID	RWL (mbgl)	Post-injection water level (mbgl)	Vertical Screen from (mbgl)	Vertical Screen to (mbgl)	Likely test section from (mbgl)	Likely test section to (mbgl)	Predominant Geodomain	Apparent hydraulic conductivity (m/sec)			
								Late time data	Mid time data	Early time data	All data
DD11OUL903	84.33	67.28	103.92	161.95	67.28	84.33	HGF	3.61×10^{-06}	4.79×10^{-07}	2.77×10^{-06}	1.86×10^{-06}
DD11OUL672	130.95	39.48	148.96	297.05	39.48	130.95	HGF	4.9×10^{-08}	7.76×10^{-08}	3.57×10^{-06}	7.79×10^{-08}
DD10OUL669	81.35	25.77	132.49	210.20	25.77	82	TRN, HGF	1.07×10^{-07}	1.44×10^{-07}	7.68×10^{-07}	1.78×10^{-07}
DD10OUL570	116	41.22	98.55	156.61	41.22	116	HGM, PHV, TRN	1.09×10^{-07}	9.04×10^{-08}	8.41×10^{-08}	9.72×10^{-08}
DD10OUL599	95.4	56.32	107.50	189.41	56.32	95.4	HGF	3.63×10^{-08}	5.84×10^{-08}	1.46×10^{-07}	6.08×10^{-08}
DD10OUL551	139.16	114.4	145.35	171.81	114.4	139.6	QTT, PHS	2.89×10^{-06}	1.53×10^{-06}	1.62×10^{-06}	1.85×10^{-06}
DD12OUL628	158.8	110.7	146.80	296.70	110.7	158.8	PHW, TRN, HGF	1.01×10^{-06}	3.17×10^{-07}	1.30×10^{-07}	6.24×10^{-07}
DD12OUL628	158.8	137.7	146.80	296.70	137.7	158.8	PHW	3.82×10^{-07}	1.61×10^{-07}	8.34×10^{-08}	1.60×10^{-07}

***Notes:*

mbgl = metres below ground level

Table F 5: Summary of well tests undertaken in Ouéléba waste rock storage facility area – 2011 to 2012 (from SWS, 2012)

Hole ID		Dominant lithology	Pump test K (m/s)	Recovery K (m/s)	Rising head test (m/s)
DD12OUL931		PHC-QTW	1.27×10^{-6}		
DD12OUL924		BAS	4.44×10^{-8}	8.6×10^{-9}	4.8×10^{-8}
DD12OUL929		BAS		1.08×10^{-8}	
DD12OUL907		BAS	5×10^{-9}		7×10^{-8}
DD12OUL908		PHS-DOL		2.193×10^{-7}	1.36×10^{-7}
DD12OUL930		DOL	1×10^{-7}		1.1×10^{-7}
DD12OUL909		QTW	3.97×10^{-9}		

Estimates of Hydraulic Conductivity by Packer Test

Table F 6: Packer tests undertaken in Ouéléba – during 2012 (from SWS, 2012)

BH ID	Test section from (m from collar)	Test section to (m from collar)	Test interval (m)	Predominant geodomain/s	Core recovery over test interval (%)	RQD (%)	Joint density	Mean permeability (m/s)	Permeability based on Lugeon response Group (m/s)	Lugeon response type	Trend of flow-pressure curves
DD12OUL629	220.25	227.25	7.00	PHW	97.2	46.2	3.6	3.8×10^{-06}	3.9×10^{-06}	D	Washout of joint filling
DD12OUL629	244.25	268.25	24.00	QTC	91.4	54.8	1.9	1.6×10^{-06}	1.4×10^{-06}	D	Washout of joint filling
DD12OUL640	202.25	250.7	48.45	QTC, PHW	93.4	50.4	2.3	4.0×10^{-08}	5.1×10^{-08}	D	Washout of joint filling
DD12OUL674	140.45	147.45	7.00	QTC	98.8	69.2	2.1	3.8×10^{-06}	3.2×10^{-06}	D	Washout of joint filling
DD12OUL674	164.45	189.85	25.40	QTC	92.3	57.3	1.7	3.5×10^{-07}	3.5×10^{-07}	A	Laminar flow
DD12OUL674	176.45	189.85	13.40	QTC	93.6	72.9	2.1	3.9×10^{-08}	3.5×10^{-08}	E	Void filling
DD12OUL676	104.9	139.15	34.25	PHS, HGF, TRN	93.3	8.5	2.8	-	-	-	-
DD12OUL676	206.75	219.75	13.00	PHC, PHV	89.8	78.6	1.1	3.3×10^{-07}	3.6×10^{-07}	D	Washout of joint filling
DD12OUL676	242.5	309	66.50	PHC, QTC, IPC	97.5	78.1	2.5	2.3×10^{-07}	2.8×10^{-07}	C	Dilation
DD12OUL677	124.4	239.3	114.90	PHW, QTW	92.8	47.3	3.0	1.3×10^{-08}	1.3×10^{-08}	C	Dilation
DD12OUL678	108.75	202.75	94.00	QTC, QTW	97.3	36.6	2.4	2.5×10^{-08}	1.7×10^{-08}	C	Dilation
DD12OUL680	66.3	83.02	16.72	PHW	95.1	71.7	1.8	5.0×10^{-09}	5.0×10^{-09}	A	Laminar flow
DD12OUL690	175.05	198.05	23.00	IPC, PHC	98.0	81.2	1.2	2.0×10^{-07}	2.0×10^{-07}	A	Laminar flow
DD12OUL690	190.05	198.05	8.00	IPC	100.0	85.5	1.5	2.4×10^{-08}	2.1×10^{-08}	D	Washout of joint filling
DD12OUL903	148.15	155.15	7.00	IPC	100.0	71.5	4.0	1.0×10^{-06}	1.0×10^{-06}	D	Washout of joint filling
DD12OUL903	154.16	161.16	7.00	IPC	100.0	61.2	6.6	3.4×10^{-08}	3.2×10^{-08}	E	Void filling
DD12OUL903	166.15	196.15	30.00	IPC, PHW	98.0	52.2	4.5	7.3×10^{-08}	7.3×10^{-08}	A	Laminar flow
DD12OUL903	178.15	196.15	18.00	PHW, PHC, QTC	98.6	55.2	4.8	2.0×10^{-08}	1.8×10^{-08}	E	Void filling
DD12OUL903	190.15	196.15	6.00	QTC, PHW, PHC	95.8	53.2	4.2	8.5×10^{-08}	8.5×10^{-08}	A	Laminar flow
DD12OUL922	308.3	369.8	61.50	IPC, PHW	98.2	43.2	4.0	1.3×10^{-08}	1.3×10^{-08}	A	Laminar flow
DD12OUL922	329.3	369.8	40.50	PHW, QTW	98.2	52.2	4.4	1.3×10^{-08}	1.3×10^{-08}	A	Laminar flow
DD12OUL922	359.3	369.8	10.50	IPC, PHC, QTW	98.6	48.4	3.0	3.1×10^{-08}	3.1×10^{-08}	B	Turbulent flow

Estimates of Hydraulic Conductivity by Particle Size Distribution

Table F 7: Hydraulic Conductivity (K) Values for Various Geodomain Codes (PSD compared to previous analysis)[29]

	PSD Analysis 2021				Previous Analysis (SWS, 2012)		
Geodomain	Count of PSD Samples	Min – Log10 K Sample (m/s)	Max – Log10 K Sample (m/s)	Geomean – Log10 K Sample (m/s)	Packer Test Geomean – Log10 K (m/s)	Injection Test Geomean – Log10 K (m/s)	Core Permeability Test Geomean – Log10 K (m/s)
TRN	7	-8.49	-2.55	-6.00		-7.57	
HGM	4	-5.49	-3.24	-4.62			
HGF	43	-7.44	-3.68	-5.23		-6.78	-8.49
PHW	9	-8.21	-5.85	-7.41	-6.86	-6.80	-7.78
CAP	7	-7.76	-2.47	-5.66			-9.43
QTZ	2	-6.92	-5.50	-6.21			
IRF	6	-6.96	-2.73	-5.08			
PHV	46	-8.93	-5.34	-7.28			-7.48
IPC	2	-6.87	-6.37	-6.62	-7.03		-8.18
QTW	28	-7.85	-5.42	-6.41			-6.89
HEF	5	-5.16	-3.62	-4.25			-3.48
PHS	15	-8.87	-6.05	-7.87			-7.28
QTZ	3	-7.85	-4.76	-5.97			
BAS	5	-8.61	-6.57	-7.61			
BAX	8	-7.34	-5.94	-6.34			
LAT	2	-7.61	-2.26	-4.93			
WEA	1	-7.06	-7.06	-7.06			
NA	239	-9.80	0.48	-5.49			

[29]Min/Max/Moyen Log10(K) Moyenne géométrique par échantillon de RGMP utilisant des méthodes pour lesquelles les critères ont été remplis pour le calcul de K – par rapport à la moyenne géométrique d'autres analyses de K antérieures utilisant des essais de remplissage, des essais d'injection et la perméabilité des carottes.

APPENDIX

G REGIONAL BASEFLOW ANALYSIS

Regional baseflow analysis

Introduction

In the 2009 flow accretion survey, a series of flow measurements were made at major confluences in the stream network at distance from Ouéléba and Pic de Fon. This was done in order to infer the contribution to the baseflow in the main rivers originating from the mountains and the distance downstream over which measurable impacts may extend. Small magnitude rainfall events were recorded in the first week of February 2009 at the end of the surveys on the mountains. These rainfall events did not affect the results and all the flow rates can be considered to be representative of baseflow.

The results of the regional survey are shown below in Table G 1, and as maps in Figure G 1 and Figure G 2.

In the table and maps, the data are shown as flow rates, catchment-normalised flow rates (i.e., flow rate divided by total catchment area – specific baseflow), and the amount of flow contributed by groundwater discharge from the mountain (shown as a percentage). Groundwater discharge from the mountain is taken as the flow rates at the boundary measurement points which are defined as the outlets of the catchments shown in Figure 8-1 to Figure 8-3 in the main report.

The mountain discharge therefore includes discharge from local aquifers on the flanks of the Pic de Fon and Ouéléba ridgelines and is not restricted to the orebody discharges alone. The contribution from mountain values are used to illustrate the relative importance of discharges from the mountain to points within the regional surface water network.

The following subsections describe what is shown in Figure G 1 and Figure G 2 in terms of the contribution of Ouéléba and Pic de Fon to baseflow in regional rivers.

The results of the regional survey are described in the context of their regional catchments; Diani, Loffa, Dion and Milo. The Diani and Loffa catchments drain much of the project area on the western and eastern sides of the range respectively, including Pic de Fon, the central ridgeline, and the southern tip of Ouéléba. The Mala, draining the western side of Ouéléba flows north into the Milo catchment. A similar pattern of drainage exists on the eastern side of Ouéléba, with the Miya draining north into the Dion catchment.

Diani catchment

The Woron, Pulowaye and Dianiworo rivers which rise on the west side of the Pic de Fon and southwest Ouéléba drain into the Soumourou River, itself a tributary of the Diani River. Above the confluence of the Woron and Pulowaye-Dianiworo rivers, the Soumourou, which drains basement rocks, had a specific baseflow of 1.8 L/s/km^2. Below the confluence of the Woron and Pulowaye-Dianiworo, specific baseflow rose to 2.5 L/s/km^2, indicating an increase of 40% in the specific baseflow of the Soumourou due to the influence of the mountains. At the confluence of the Woron with the Soumourou, approximately 73% of the baseflow in the Soumourou was estimated to originate from Ouéléba and the northwest flanks of Pic de Fon.

A short distance below the confluence of the Woron River with the Soumourou, the Soumourou is also joined by the Pulowaye-Dianiworo River in which the baseflow was 152 L/s. At this point, 77% of the flow in the Soumourou originated from Ouéléba and Pic de Fon. Together the Woron and the Pulowaye-Dianiworo contributed 12 L/s/km^2 to the Soumourou.

Downstream, the Soumourou flows into the Diani River which flows southward. The yield of the Diani was raised by 29% (834 L/s) at the confluence of the Soumourou. Upstream of the confluence, 79% of the baseflow in the Soumourou is attributed to the mountain tributaries (Woron and Pulowaye-Dianiworo) from Ouéléba and Pic de Fon. This reduced to about 18% in the Diani downstream of the Soumourou-Diani confluence owing to a substantial contribution from the Diani River, equivalent to 4.2 L/s/km^2, intermediate to that of the mountain and basement aquifers, probably owing to the headwaters of the Diani being situated in the wetter upland areas to the west of Simandou.

At the confluence of the Kouankan tributary with the Diani the contribution of the mountain is maintained at nearly 18%, the balance being contributed by flow from the highlands to the northwest.

The Fokou West River, which drains the southwest flanks of Pic de Fon, is a tributary of the Diani River. At the downstream measurement point on the Fokou West River, 39% of the flow originated from Pic de Fon and specific baseflow was 2.9 L/s/km^2, similar to the Dianiworo River at its confluence with the Pulowaye.

South of the Simandou range the Diani River is joined by the Loffa which drains the southeast flanks of Ouéléba and the eastern flanks of Pic de Fon. The flow at Bac Diani, the government gauging station downstream of the confluence was not measured during the survey; however, from long-term records at Bac-Diani (1976-2006) the mean monthly flow in February is 15.61 m^3/s or 3.8 L/s/km^2, indicating that its specific baseflow is maintained from Kouankan to Bac-Diani. This is largely owing to the influence of the Simandou range.

Loffa catchment

The Loffa drains the southeast flanks of Ouéléba and the eastern flanks of Pic de Fon. A flow of 161 L/s and the highest specific baseflow in the upper Loffa catchment of 14.8 L/s/km^2 was measured upstream of Canga East Road crossing. At this location, about 94% of flow originated from Ouéléba and Pic de Fon.

As it flows south, the Loffa receives inflows from tributaries draining the eastern flanks of Pic de Fon and from tributaries draining hills to the east. Specific baseflows in south eastward draining mountain catchments ranged from 3.7 L/s/km^2 (Whisky 4 River) to 6.8 L/s/km^2 (Whisky 1 River). The Loffa River gained flow between the Canga East Road and Foma Village. Overall specific baseflow at Foma was 6.6 L/s/km^2. At Foma it was estimated that 33% of the flow originates from the mountain, suggesting substantial contributions from left bank tributaries.

A left bank tributary entering the Loffa upstream of Foma had a specific baseflow of 3.4 L/s/km^2, indicating that the non-mountain catchments to the east which drain hilly country underlain by basement rocks have a lower yield than the mountain catchments. Similar specific baseflows of 2.8 L/s/km^2, 3.9 L/s/km^2 and 4.8 L/s/km^2 were obtained in three northward draining catchments east of Nionsonmoridou.

No measurements were made downstream of Foma; however, the flow in the Loffa is expected to gain slowly as it flows south, receiving right bank tributaries from the southern Simandou range. To the south of the Simandou range, the Loffa flows into the Diani.

Dion catchment

The specific baseflow on the Miya River at Siatouro was 8 L/s/km^2, fairly typical of mountain catchment yields. At this point, about 54% (i.e., the majority) of the flow was estimated to originate from Ouéléba.

Further north at Nionsonmoridou, flow in the Miya increased but specific baseflow fell slightly to 6 L/s/km^2 and the contribution from Ouéléba also fell slightly to 50%. This percentage contribution is lower than westward draining tributaries, but similar to southeastward draining tributaries in the Loffa catchment.

No measurements were made to the north of Nionsonmoridou, but flow records at Baranama on the Dion (2000-2006) show the mean flow in February is 51.7 m^3/s, equivalent to 7.8 L/s/km^2. This indicates that the Dion maintains a relatively high specific baseflow, probably as a result of left bank tributaries draining from the Simandou range along its length.

Milo catchment

The Mala River drains northward to the Milo. The Mala gained substantial flow along its course between Traorela and Moribignedou. Specific baseflow at Traorela was 5.9 L/s/km^2. This was maintained to Moribignedou where it was 5.8 L/s/km^2. These values are comparable to the specific baseflow at Nionsonmoridou. Approximately 89% of the flow at Traorela was estimated to originate from Ouéléba, falling to 16% at Moribignedou.

No measurements were made to the north of Moribignedou, but flow records at Konsankoro on the Milo (1979-1989) show the mean flow in February is just 3.7 m^3/s, equivalent to 3.7 L/s/km^2, suggesting that the Milo gains flow only slowly and probably loses flow along reaches of its course.

Table G 1: 2009 streamflow rates at regional measurement points

Location	X	Y	Flow (L/s)	Catchment Normalised flow (L/s/km^2)	Contribution from mountain* (%)
Diani					
Woron-1	505198	949104	682.9	14.9	76
Woron-2	503029	947513	667.7	13.0	78
Woron-3	497282	944628	644.8	10.0	81
Pwaye-1	503098	944461	88.4	8.7	73
Pwaye-2	499734	943337	74.2	2.8	87
Dworo-1	503190	940873	56.4	2.4	139
Dworo-2	499839	942732	79.4	2.9	99
Dworo-3	497191	944195	152.0	2.1	94
Smarou-1	503965	956037	106.9	6.8	0.0
Smarou-2	503065	953355	109.3	3.5	0.0
Smarou-3	500935	951830	124.7	3.3	0.0
Smarou-4	497963	949507	240.2	1.8	0.0
Diani-1	492379	940213	2,884.4	4.2	0.0
Diani-2	492453	939595	3,718.6	3.7	18
Diani-3	489822	929503	3,743.2	3.4	18
Seia-1	489035	929974	132.5	1.4	0.0
Vele-01	503554	928232	24.1	1.3	0.0
Fokou_W-1	503471	929635	705.8	9.9	28
Fokou_W-1	494297	929365	503.5	2.9	39
Loffa					
Loffa-01	514611	949229	161.2	14.9	94
Loffa-02	515817	949266	221.2	7.0	68
Loffa-03	517444	941326	234.3	3.7	65
Wsky1-01	515100	943760	63.0	5.8	112
Wsky4-01	515754	941973	82.3	6.8	94
Wsky1-02	515780	942040	66.8	5.3	105
Wsky1-03	517293	941184	108.4	6.0	145
Loffa-04	517979	940644	454.3	5.0	68
Loffa-05	518606	939383	589.2	3.9	52
Loffa-06	518441	937614	964.1	6.6	33
Boe	518620	937679	42.7	4.1	33
Loffa-trib	518089	940757	202.4	3.4	0.0
Dion					
Miya-02	517155	963948	277.8	6.0	50
River1	522814	964541	288.9	2.8	0.0
River2	529626	963629	411.6	3.9	0.0
River 3	529328	963343	65.4	4.8	0.0
Milo					
Mala-02	505290	969944	780.1	5.8	16

* % of total groundwater discharge from mountain as defined by boundary measurements

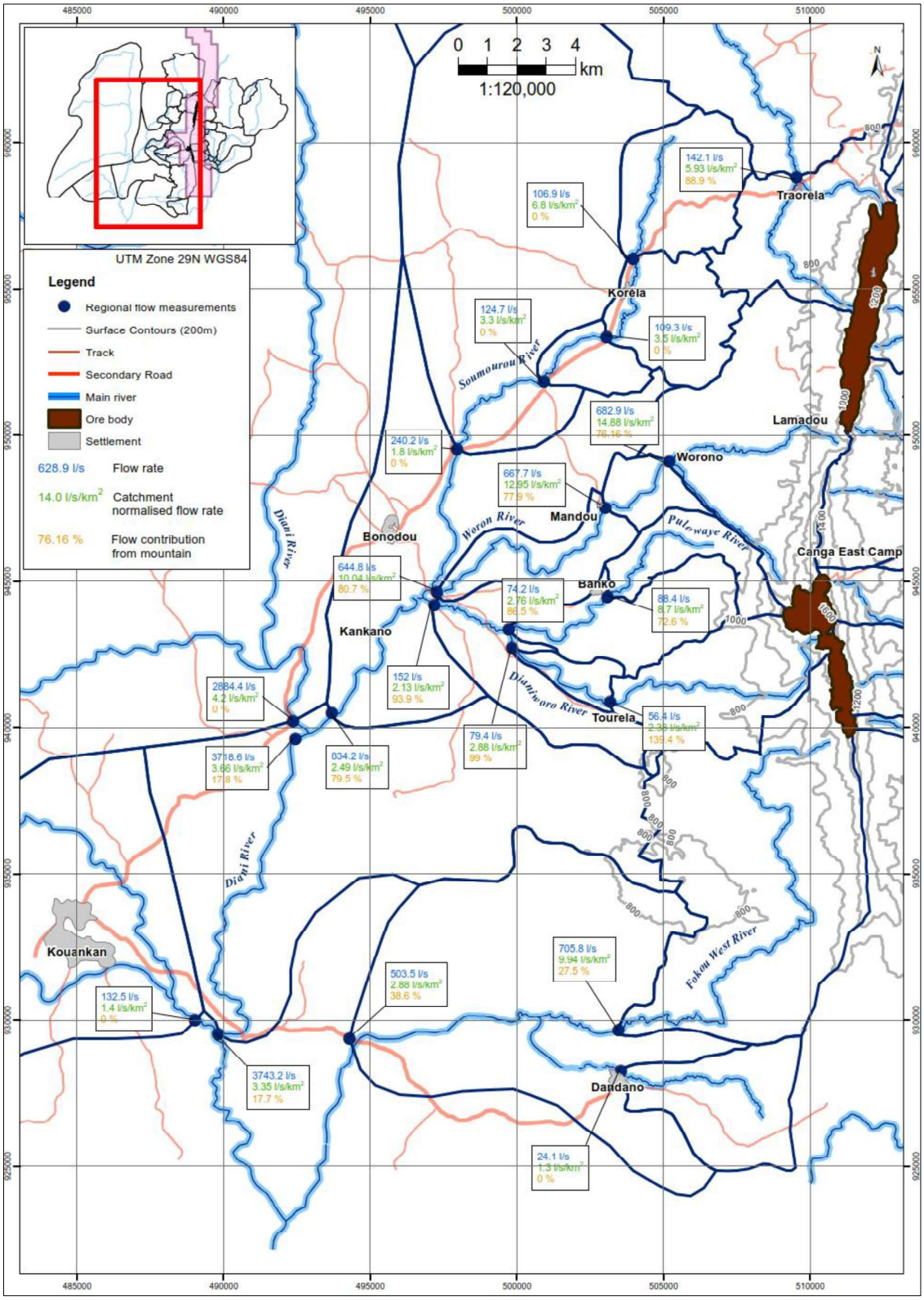

Figure G 1: 2009 streamflow rates at regional measurement points; west of Simandou (from SWS, 2012)

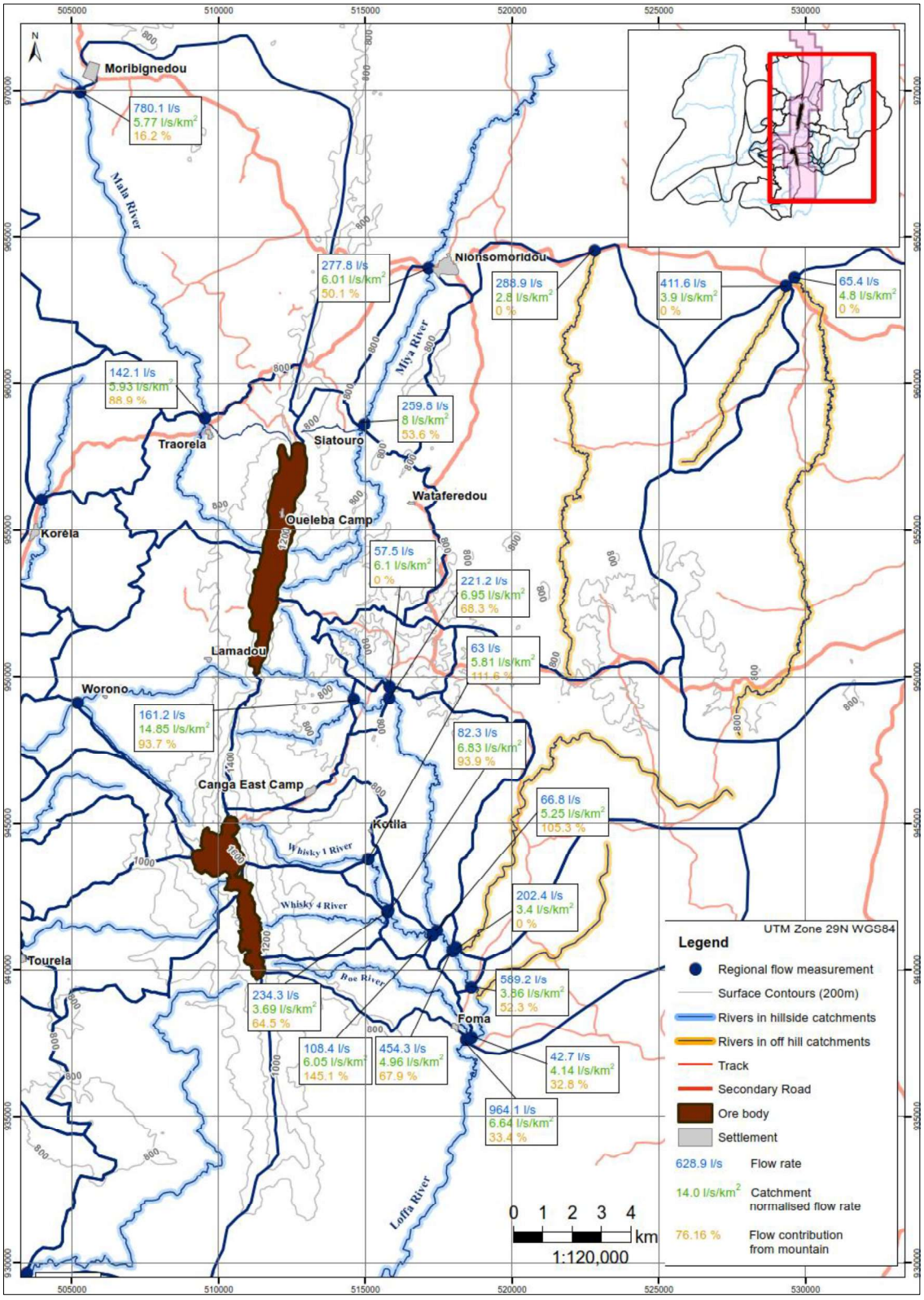

Figure G 2: 2009 streamflow rates at regional measurement points; east of Simandou (from SWS, 2012)

APPENDIX

H STABLE ISOTOPE STUDY

Stable Isotope Study: Methodology

Stable isotope data was collected as part of the 2022 dry season baseline monitoring programme at a total of 61 springs and stream locations. All samples are considered representative of baseflow conditions. Isotope data was also collected from spring and stream locations during sampling in March 2012 (SWS, 2012), with samples from Pic de Fon as well as from Ouéléba. The 2012 dataset is also considered broadly representative of baseflow conditions, although 4 of the 10 samples were collected on 2nd March 2012 following heavy overnight rain so some dilution of baseflow with surface runoff cannot be ruled out.

Duplicates were undertaken in both the 2012 and 2022 campaign and several repeat samples were also taken:

- A single duplicate sample was collected during the 2012 sampling campaign and showed a relative percent difference (RPD) between the normal and duplicate of 5.5%.
- Two duplicates were collected during the 2022 campaign, and both showed RPD's of less than 5%.
- Five repeat samples were also collected during the 2022 campaign and showed very little variance with RPD's all less than 5%. The period between repeat samples was in the order of one month for all samples.

Four of the sites sampled in 2012 were also sampled in 2022. Two of the sites were weir locations so there is high confidence that the exact location was resampled. The stream sampling sites (on the Boyboyba and Kinyeko) may have differed by several 10's of meters but this is unlikely to have impacted the results. RPD's of between 5 and 7% were recorded at three of the sites. The fourth site, Whisky 5 Weir, showed a larger RPD of 16% which may be attributable to heavy overnight rainfall prior to the 2012 sampling event.

Overview of Stable Isotope Behaviour and its importance to Simandou

Hydrogen can occur as two stable isotopes: 2H and 1H, where the 2H isotope includes an extra neutron. Oxygen primarily occurs as the 16O isotope but may also occur as 17O or 18O due to the presence of additional neutrons. Whilst 2H and 18O only comprise a small fraction of the overall hydrogen and oxygen occurring in water molecules, analytical methods can determine the difference. This is measured relative to standards, typically the Vienna Standard Mean Ocean Water (VSMOW) for water molecules. Measurements are therefore reported as parts per thousand (ppt or ‰) relative to the VSMOW value.

The higher mass of the heavier isotopes means that the 2H and 18O behave slightly differently than the corresponding 1H and 16O isotopes, resulting in fractionation between the water during evaporation and precipitation. Lighter water molecules will preferentially be evaporated, so that water vapour tends to be depleted in 2H and 18O relative to the liquid water source, and conversely, the liquid water is effectively enriched by the preferential evaporation (removal) of the lighter isotope molecules.

Similarly, heavier water will preferentially condense and form precipitation, such that precipitation becomes increasingly depleted with distance from the source (or the coast, in the case of Simandou) and increasing elevation. It is this elevation control on isotope depletion that is particularly relevant at Simandou because the orebody is recharged by rainfall falling at higher elevations (*i.e.* on top of the ridgeline).

When assessed on a global basis, stable isotope values for water within clouds and rainwater sourced from the seas and oceans typically fall along a typical range, called the Global Meteoric Water Line (GMWL). The GMWL is an average of many local and regional meteoric water lines which differ from the GMWL due to varying climatic and geographic parameters (Clark & Fritz, 2013).

Establishing a representative local meteoric water line (LMWL) is desirable for accurate interpretation of isotope data but several years of seasonal data is required to achieve this. In the absence of local data, the Global Network of Isotopes in Precipitation[30] (IAEA/WMO, 2022) provides an online database of regional data that can be used to support local isotope studies.

Figure H 1 summarises the different effects and processes which may act to change the isotopic signature of the waters (Clark & Fritz, 1997). Evaporation is the main process that commonly gives rise to fractionation, but this process is most applicable in arid climates. Whilst the evapotranspiration at Simandou is high, the majority is attributable to transpiration. Transpiration is a non-fractionating process as water is taken up in roots and released through the stomata; there is no mechanism for preferential evaporation of the lighter water molecules (Clark & Fritz, 1997).

Several of the processes shown in Figure H 1 are less likely to occur at Simandou, particularly the high temperature exchange of rock minerals and the H_2S exchange. Hydration of silicates and low temperature exchange with rock minerals are possible but tend to require longer (geological) timeframes to have a discernible influence. These elevated residence times are not anticipated at Simandou where aquifer residence times are in the order of years or decades. The process of CO_2 exchange may occur, but this process is rarely observed in nature.

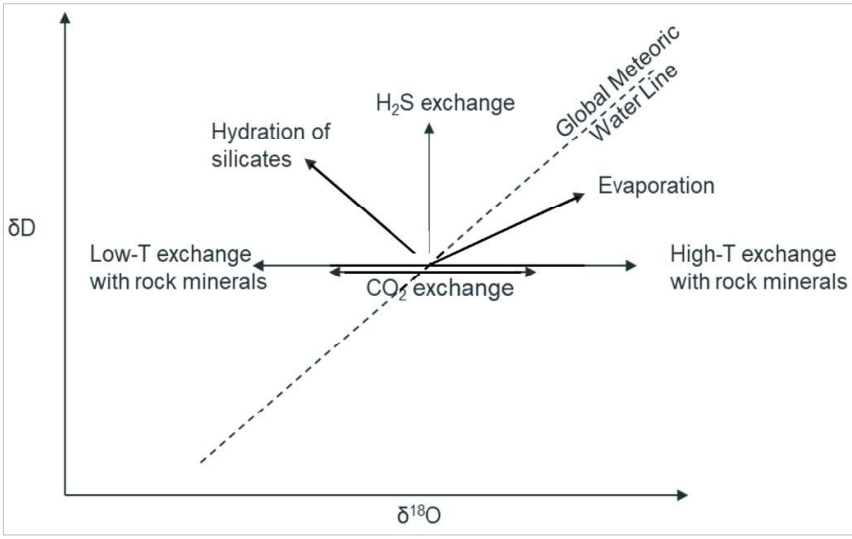

Figure H 1: Schematic of stable isotope fractionation processes

[30]Le réseau mondial d'isotopes dans les précipitations (GNIP) a été créé par l'Agence internationale de l'énergie atomique (AIEA) en collaboration avec l'Organisation météorologique mondiale (OMM). Il fournit une sélection mondiale de stations météorologiques où des échantillons sont prélevés pour surveiller la composition $^{18}0/^{2}H$ des précipitations.

Both 2012 and 2022 results are shown on the graph in Figure H 2 below

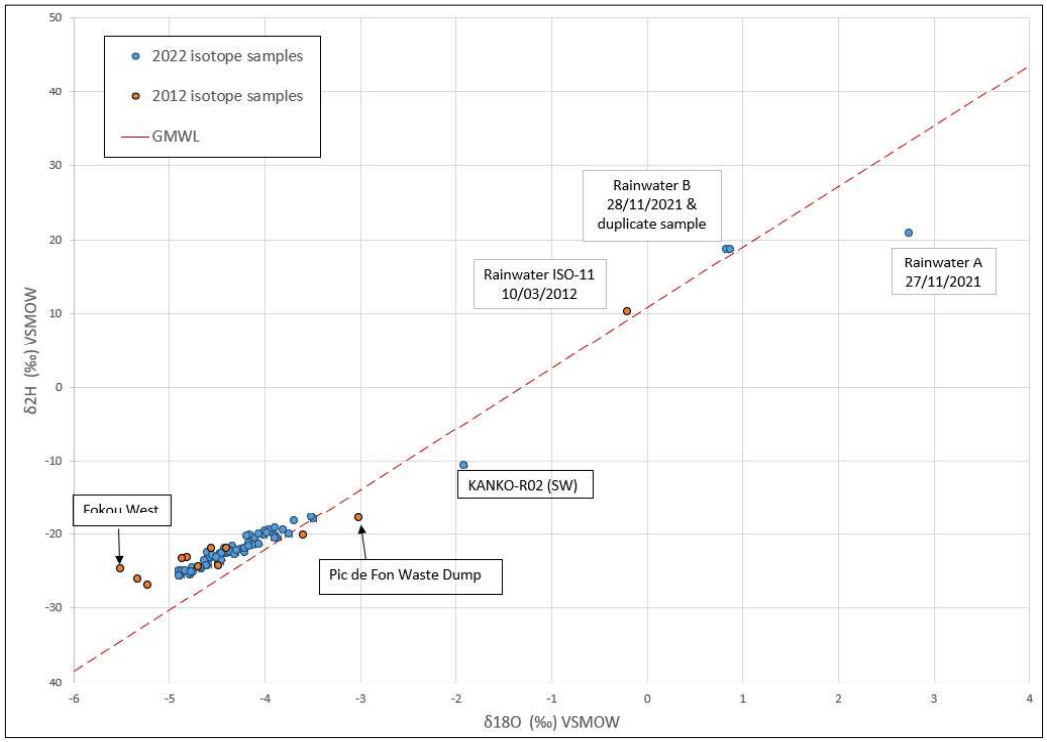

Figure H 2: Combined (2012 & 2022) Simandou $\delta^{18}O$ / $\delta\ ^{2}H$ results

Figure H 2 shows that most samples follow a linear trend just above the GMWL and plot within a relatively narrow range from -5.5‰ to -3‰ for $\delta^{18}O$ and -26‰ to -18‰ for $\delta^{2}H$. Samples from Pic de Fon (taken in 2012) show greater depletion with the lowest concentration observed at the Fokou West spring, the primary discharge point of the southern Pic de Fon ore body. The most enriched sample was reported at the proposed waste dump location on the basement plain to the south-east of Pic de Fon.

An outlier is observed at KANKO-R02 which is situated on basement geology to the northwest of Ouéléba. This location was reported as stagnant with no flow. The sample is considered unrepresentative of baseflow and has almost certainly been enriched by open water evaporation.

Comparison of $\delta^{18}O$ / $\delta^{2}H$ in Surface Water and Precipitation

Figure H 2 shows a large offset between the spring and surface water samples and the site rainfall data. Regional GNIP datasets have been interrogated to explain the discrepancy and they show significant seasonal variability in the composition of rainfall. Table H 1 presents precipitation data for Bamako in Mali which has a (discontinuous) 56-year record of $\delta^{18}O$ / $\delta^{2}H$ concentrations running from 1962 to 2018. Depletion is greatest in the wettest months (July – September) and lowest in the drier months. The rainfall samples collected at the Simandou site are taken from March 2012 (at the start of the wet season) and November 2021 (at the end of the wet season) and would therefore be expected to show lower depletion.

Figure H 3 shows the monthly distribution of $\delta^{18}O$ concentrations reported in the GNIP database for West Africa along with those measured in site rainfall. The site rainfall data is within the observed range for the months they were collected. The seasonality is attributed to enrichment of rainfall during drier months as the lighter component is removed by atmospheric evaporation of moisture.

The potential for atmospheric enrichment is lower in the wet season due to the prevalence of the moister monsoon air masses and lower atmospheric evaporation. The range of concentrations observed in Simandou spring and surface waters are also consistent with the measured wet season rainfall concentrations[31] as indicated on Figure H 3.

The site rainfall samples collected in November 2021 show a large difference in composition of rainfall samples taken on consecutive days. Evapo-concentration of the sample in the manual rain gauge at Canga East was unlikely to have occurred as samples were bottled shortly after the rainfall event.

Significant short-term variations in rainfall composition are common and “rainout” of the heavier isotopes typically occurs during individual events; Clark & Fritz report $\delta^{18}O$ concentrations ranging from -3‰ to less than -6‰ during a single 12-hr storm event for example.

Comparison of Simandou rainfall data with the GNIP[32] data set (Figure H 4) also illustrates that site rainfall data is within the range of regionally observed values. All site rainfall data is therefore considered reliable.

Figure H 4 presents the site data relative to West African country specific LMWL’s, a regional MWL and the GMWL. The Simandou samples plot in a similar area of the graph, slightly above the GMWL and Regional MWL. The Benin country specific water line is very closely matched to the Simandou samples suggesting this may be the closest match to precipitation composition at Simandou. The GNIP database contains no data for Guinea itself or its immediate neighbours in southern Guinea (i.e., Ivory Coast, Liberia, Sierra Leone).

[31]Le calendrier précis de la saison des pluies varie légèrement dans la région ; les mois de juillet, août et septembre sont considérés comme les principaux mois de la saison des pluies aux fins de cette comparaison.
[32]Le Réseau mondial des isotopes dans les précipitations (GNIP) est un réseau mondial de surveillance des isotopes de l'hydrogène et de l'oxygène dans les précipitations, lancé en 1960 par l'Agence internationale de l'énergie atomique (AIEA) et l'Organisation météorologique mondiale (OMM), et fonctionnant en coopération avec de nombreuses institutions partenaires dans les États membres.

Table H 1: Seasonal variation in precipitation and $\delta^{18}O$/ $\delta^{2}H$ concentrations for Bamako, Mali (IAEA/WMO, 2022)

	Precipitation [mm]		$\delta^{18}O$ [‰]		$\delta^{2}H$ [‰]		d-excess [‰]		Air Temp. [°C]		VP [hPa]	
Month	Avg	n	Avg	n	Avg	n	Avg	n	Avg	n	Avg	n
January	0.1	30	-	0	-	0	-	0	25.1	30	8.3	24
February	0.3	30	8.22 ± 1.89	3	41.2 ± 19.2	3	-24.5 ± 9.3	3	28.0	30	8.3	24
March	3.7	29	4.78 ± 3.06	5	22.3 ± 8.7	4	-8.2 ± 13.4	4	30.4	29	10.2	24
April	22.6	30	2.26 ± 3.11	12	16.0 ± 22.4	10	-2.4 ± 7.2	10	31.9	30	16.4	24
May	53.4	29	-0.03 ± 3.16	16	3.4 ± 21.1	16	3.7 ± 6.7	16	31.1	30	22.3	24
June	122.3	30	-2.28 ± 1.74	23	-9.1 ± 11.8	23	9.2 ± 5.0	23	28.7	30	25.4	24
July	213.7	29	-4.91 ± 2.33	23	-34.1 ± 16.4	21	8.5 ± 4.0	21	26.5	29	26.4	23
August	260.9	29	-6.58 ± 2.23	22	-45.4 ± 15.1	21	8.8 ± 4.9	21	25.8	28	26.7	23
September	197.5	28	-3.69 ± 2.73	23	-26.8 ± 13.8	21	5.3 ± 8.8	21	26.3	28	26.4	23
October	70.2	30	-2.44 ± 3.24	16	-14.4 ± 19.0	16	5.2 ± 10.6	16	27.4	30	23.9	24
November	3.1	30	2.70 ± 2.64	4	19.7 ± 20.3	4	-1.9 ± 4.4	4	26.5	30	14.4	24
December	0.8	30	-0.3	1	6.8	1	9.2	1	24.9	30	10.0	24

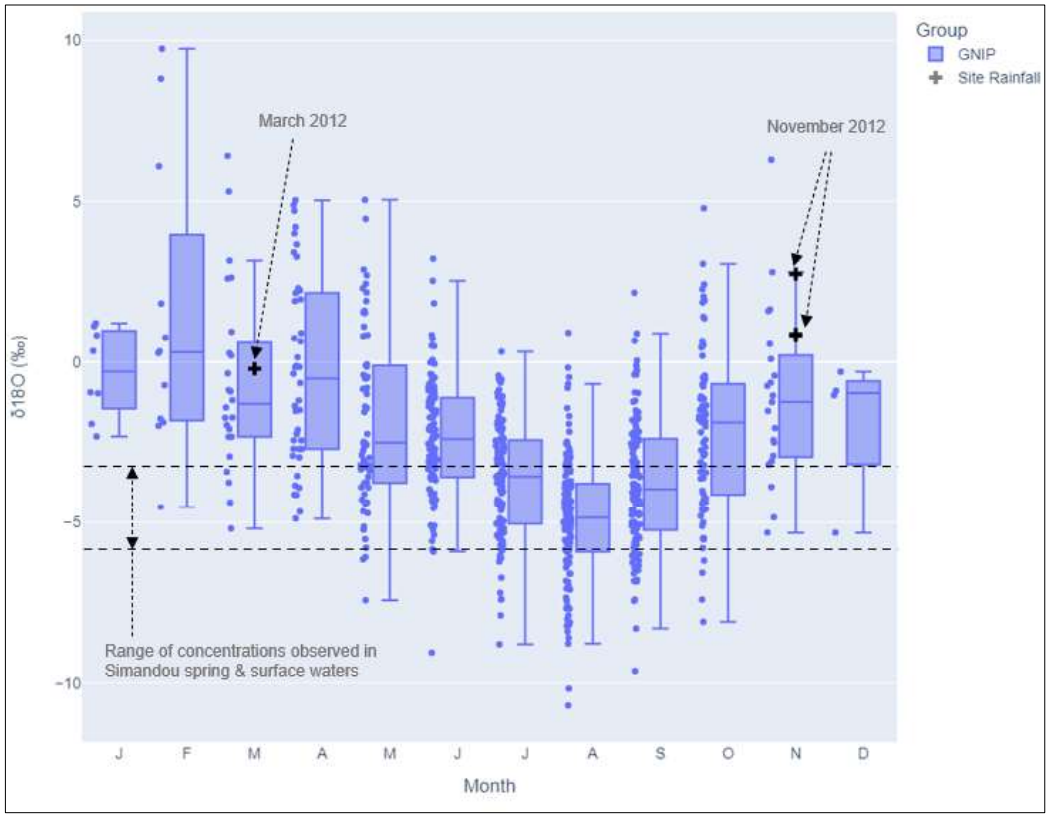

Figure H 3: Month vs $\delta^{18}O$ for GNIP (West Africa) samples and Site Rainfall

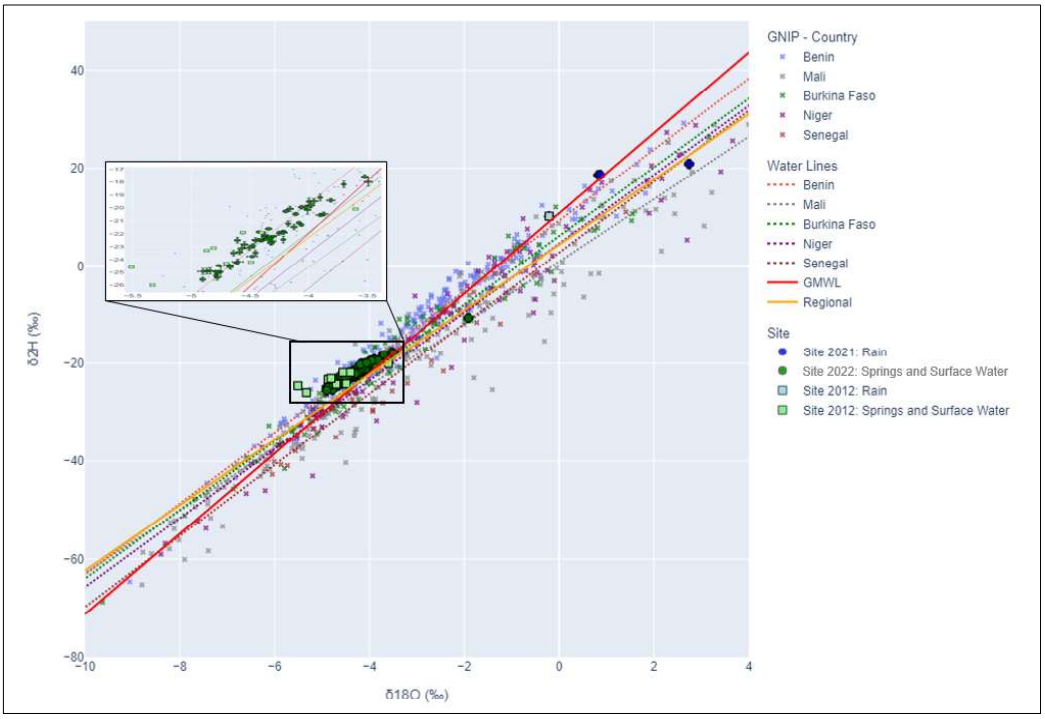

Figure H 4: Simandou isotope results relative to GNIP data and country-specific LMWL's

Seasonal Variability and Impact on Groundwater Composition

The range of stable isotope concentrations observed in spring and surface water samples at Simandou is far smaller than that observed in the GNIP precipitation database. This limited range is attributed to all samples being representative of groundwater composition, given that they were collected during the dry season with little or no impact from surface water runoff events.

Clark & Fritz (1997) note that groundwaters in temperate climates typically show an isotopic value that is close to the weighted average of annual precipitation. It is considered that the same will be true in tropical environments such as Simandou due to the lack of fractionation during transpiration, and is evidenced by the observed range of Simandou samples relative to regional GNIP data shown in Figure H 5.

Clark & Fritz (1997) also describe the critical depth 2σ, defined as the point below which variability is less than the analytical precision (Figure H 5). Critical depths range from 3 to 5m in fine grain soils with limited preferential flow pathways to several 10's of metres for fractured rock environments.

In the context of the Simandou orebody, groundwaters are expected to show limited seasonal fluctuation due to the large unsaturated zone and additional attenuation within the aquifer itself. Seasonal and interannual variability is more likely on the flanks of the ridgeline where both unsaturated zone thickness and aquifer volume is lower.

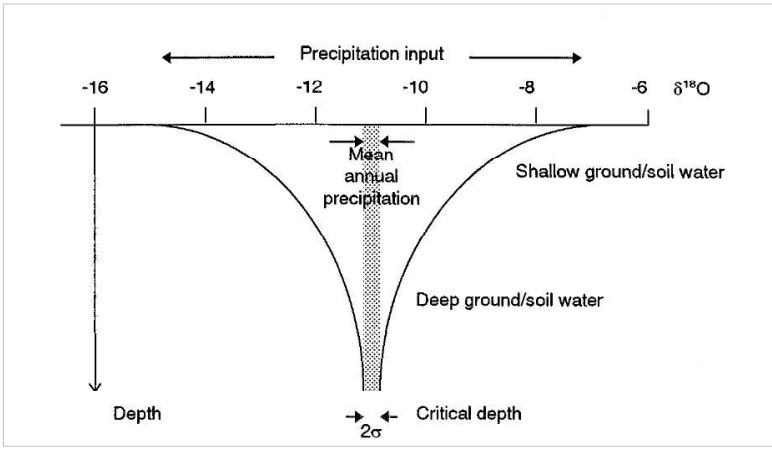

Figure H 5: Schematic of attenuation of seasonal isotope variations within the unsaturated zone (from Clark & Fritz, 1997)

Altitude Effect on $\delta^{18}O$/ $\delta^{2}H$ Depletion

The correlation between altitude and $\delta^{18}O$/ $\delta^{2}H$ depletion is well documented in the literature and is explained by adiabatic cooling of the air mass and subsequent rainout of heavier isotopes. Whilst some countries have published altitude – depletion relationships, no such relationships have been derived for Guinea or its immediate neighbours.

The closest relevant dataset is from a detailed analysis of altitude effects on Mount Cameroon (Fontes and Olivry, 1977) where a gradient of -0.155‰ $\delta^{18}O$ per 100-m rise in elevation was derived. Clark & Fritz (1997) give a range of -0.15 and -0.5‰ $\delta^{18}O$ per 100-m rise in altitude based on eight published case studies and observe that the shallow gradient on Mount Cameroon is due to the low temperature gradient.

Clark & Fritz (1997) state that the altitude effect is: "*useful in hydrogeological studies, as it distinguishes groundwaters recharged at high altitudes from those recharged at low altitude. The effect is observed even in watersheds with elevation contrasts of less than a few hundred metres, provided that sufficient data are collected to resolve seasonal effects*."

In the case of Simandou the altitude range over the area of interest is approximately 1,000m and the seasonal effects are limited for groundwaters in the orebody for the reasons described above.

All site rainfall data has been collected at the Canga East rain gauge so no data is available to evaluate the impact of elevation on rainfall composition at Simandou. The large variability in rainfall composition (both short-term and seasonal) will also make derivation of a site-specific altitude – depletion relationship impossible without an extensive data set from rain gauges at multiple elevations and extending over a period of at least 2 years.

In the absence of a site-specific rainfall data set it is possible to infer an elevation – depletion relationship from available surface water samples. Figure H 6 presents the elevation of collected samples against $\delta^{18}O$ depletion for all 2022 dry season samples. As a general pattern, the results show the samples from the lower elevations are the least depleted (most positive), and that the most depleted isotope values (most negative) are associated with the smaller springs and flows from higher up the ridgeline. This is to be anticipated given that depletion is primarily a function of the elevation at which the groundwater recharge occurred.

Figure H 6 also shows multiple samples where higher levels of depletion are observed at lower elevations. This reflects the fact that surface water samples represent a blend of waters recharged upstream of the sampling point. This point is best illustrated by comparing the individual data points with the inferred precipitation $\delta^{18}O$ – elevation relationship for the project area. This inferred relationship is based on the results of both the 2012 and 2022 sampling campaigns and an assessment of the groundwater catchments for a selection of sampled points and is shown as a zone rather than a discrete line due to its uncertain nature.

In theory, all sampled points should sit on or below the $\delta^{18}O$ – elevation line. Samples resting on or close to the line represent those that are collected at a similar elevation to where those waters were recharged. Samples showing a significant offset below the line indicate the predominance of flows recharged at higher elevations, which in the case of Simandou would also represent those streams fed by the orebody aquifer.

The value of the depletion-elevation relationship as a means of identifying the groundwater source is partly driven by the repeatability of the readings. The review of duplicate data, repeat readings and the comparison of 2012 and 2022 datasets presented above illustrated that repeat readings were consistently within +/- 5% except for one sample that was likely impacted by overnight rainfall. A 5% error margin equates to an elevation differential of between 50 and 100m for the range of $\delta^{18}O$ concentrations observed in Simandou surface waters.

Further interpretation of isotope distribution is presented below.

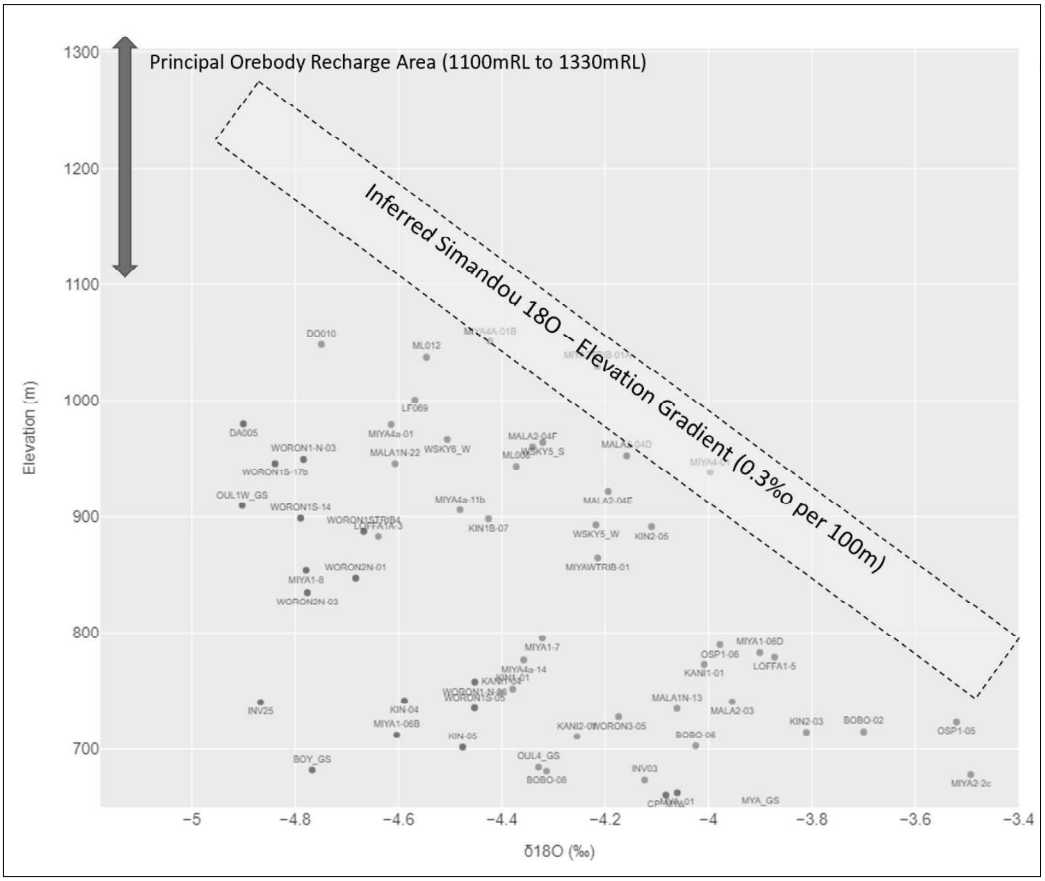

Figure H 6: Relationship between site sample elevations and $\delta^{18}O$ depletion

Delineation of Orebody Discharges using $\delta^{18}O$ / $\delta^{2}H$ Isotopes

As discussed in above the δ18O / δ2H depletion reflects the elevation at which groundwater recharge occurred, and the fact that the orebody aquifer is recharged at higher elevations along the ridgeline means that greater depletion is anticipated, relative to groundwaters recharged on the flanks of the mountain or the lowland plains. The isotope data must however be interpreted alongside other hydrogeological datasets to draw meaningful conclusions on connections between the orebody aquifer and surface waters.

Figure H 7 presents a spatial plot of oxygen isotope values for the dry season samples. The data is presented alongside EC and flow rate data from the 2022 dry season flow accretion and water quality survey. As discussed in Chapters 6 and 8 in the main report, EC and flow rate data are also used as indicators of orebody discharge locations.

In addition to the conceptual interpretation presented in Section 7.3 of the main report text, the δ18O depletion data also has potential to determine the proportion of orebody discharges in surface waters extending downstream if supplemented with additional data from lowland streams and groundwater samples. Figure H 8 provides an example from north-east Ouéléba where the more depleted MIYA1-8 spring waters are seen to be the primary control on the sample obtained downstream at the Boyboyba gauging station (BOY_GS).

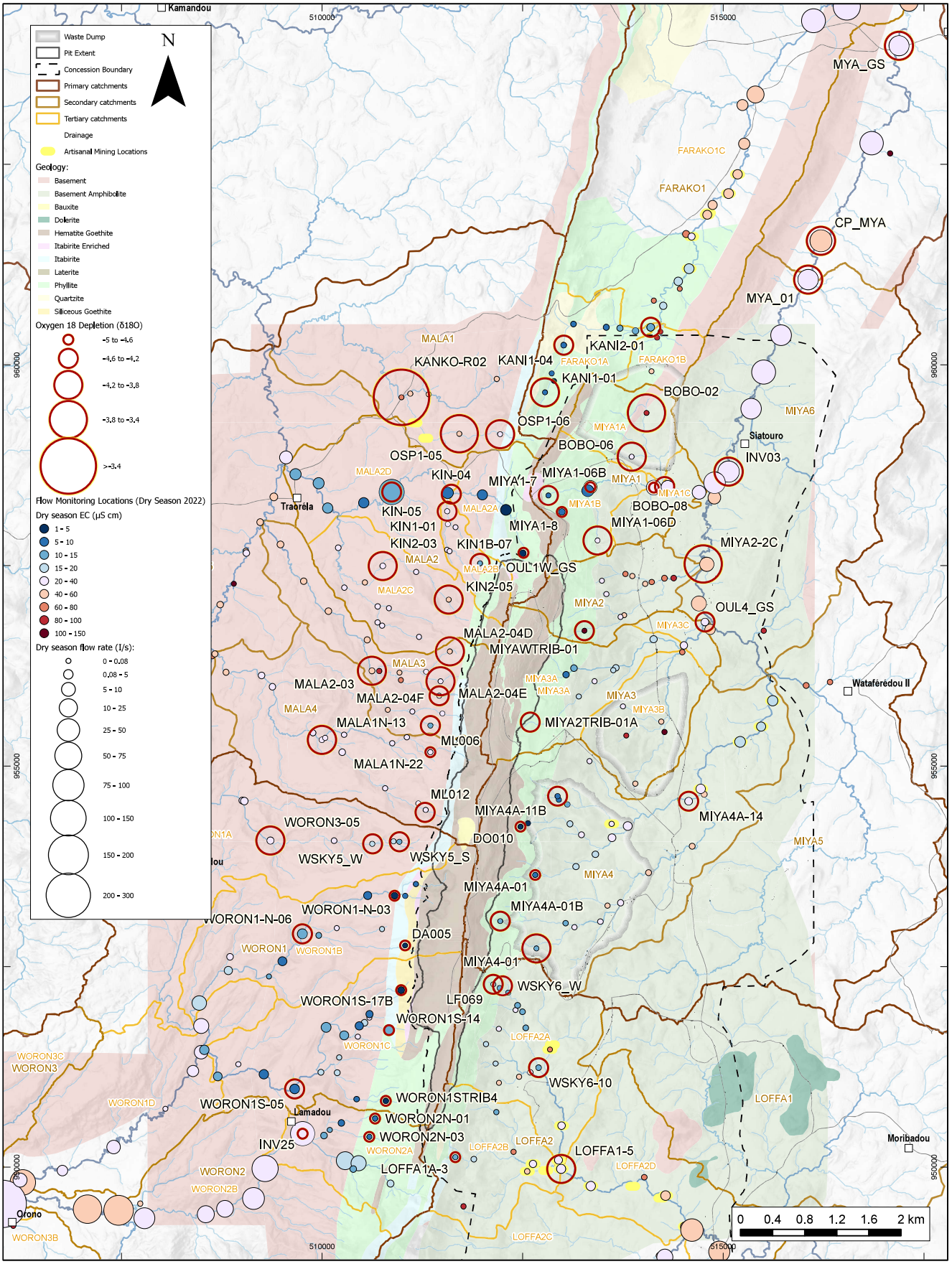

MARCH 2023	31243	SIMANDOU GEOTECH AND HYDRO BFS	
srk consulting		Dry season 2022 monitoring locations: Oxygen 18 Depletion, Flow rates and Electrical Conductivity	Figure H-7

E:\SRK Consulting\UK 31243 Simandou Geotech and Hydro BFS - General\03_Reference\FigureWorkspaces\BaselineGW_IsotopeFlowEC_20230301.aprx

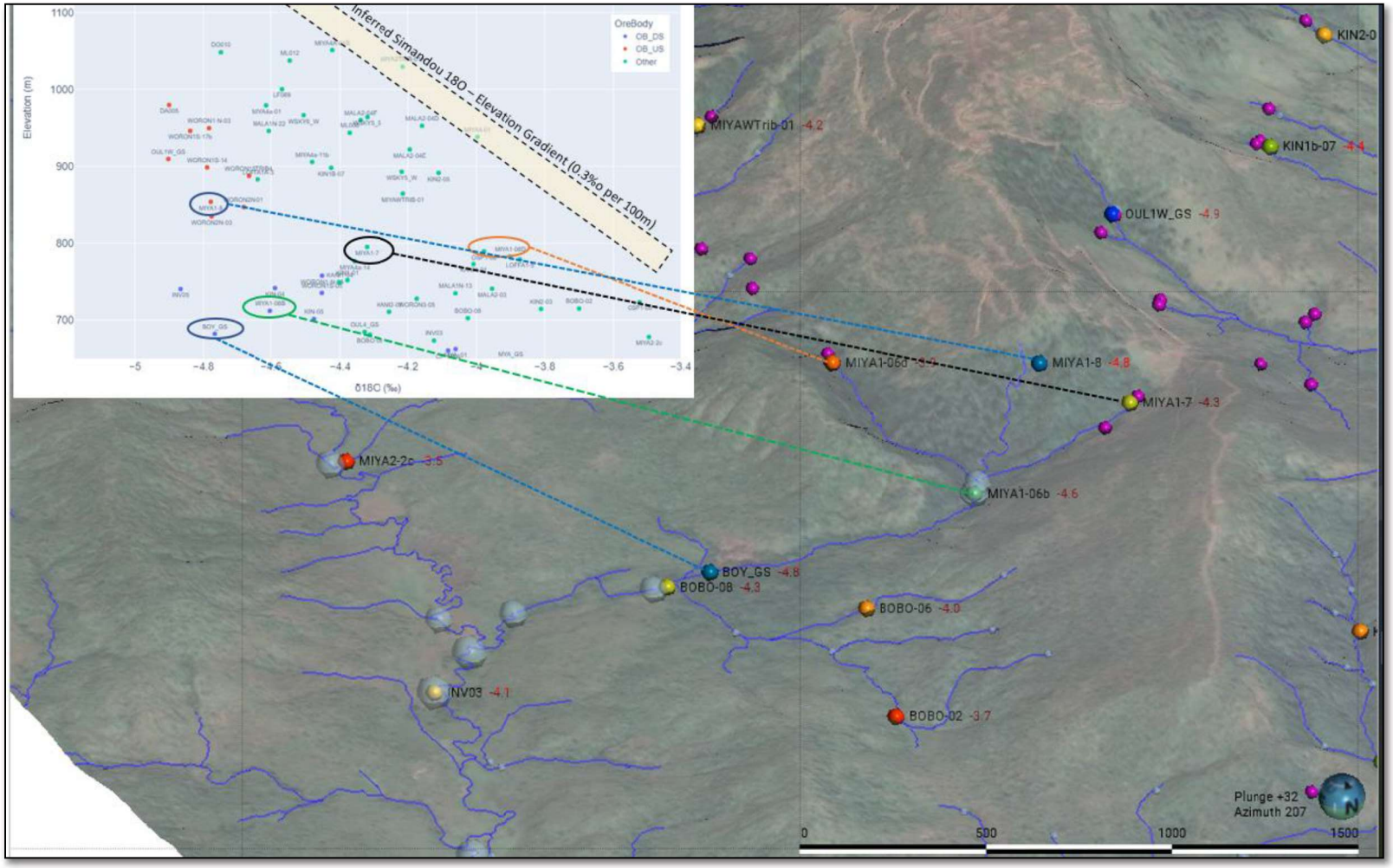

Figure H 8: δ18O concentrations downstream of ore body discharges in north-east Ouéléba

APPENDIX

I PIC DE FON GROUNDWATER SURFACE

PIC DE FON GROUNDWATER SURFACE

Approach

All groundwater level data has been interpreted in the context of the conceptual model detailed above. The groundwater surface for Pic de Fon was generated by SWS (2012) with a 3D surface modelling tool[33] which allows the user to shape a gridded surface as required to fit the water level data and geological structure. In this way, the groundwater contours can be generated from the gridded surface so that accurate small-scale detail is retained.

The following limitations are inherent in this process, and these should be considered when reviewing the groundwater level surfaces:

- The grid spacing used for modelling the groundwater level surfaces (10 m x 10 m) implies a level of accuracy which cannot be attained through qualitative interpretation of the available data. Fine gridding is however necessary to fit the groundwater surface to known structural controls. The groundwater level surfaces are thus interpretive, particularly in areas where groundwater level data are sparse or non-existent.
- The groundwater level monitoring data indicates significant variation in groundwater levels in some lithologies. Representative groundwater levels have been selected from the monitoring dataset to guide the modelling of the groundwater surface, hence not all of the groundwater level data imported into Petrel are fitted exactly to the groundwater surface. This is an essential part of the process as interpretation and judgement is required to delineate between perched water tables and those representative of the deeper groundwater surface.
- The modelled groundwater surface has been prepared to be representative of groundwater surfaces and gradients. The water table surface has been created in 3D using the Petrel surface modelling tool which incorporates an operation to smooth out irregularities in the surface. In some areas, smoothing has resulted in groundwater gradients which do not reflect expected Darcian type head distributions along certain flow paths.
- The groundwater surface has been modelled as a single and continuous groundwater body. In reality there are perched water tables present above the groundwater surface.

A series of Petrel screenshot images are included in Figure I 1 to Figure I 3 to illustrate the process for the Northern and Central Zones on Pic de Fon. The process shown in these figures and documented below has been followed over the full length of both deposits.

The contoured surface shown on the screenshots represents the water table. Geology sections from the resource block models are also shown and the geology shown includes the various orebody and itabirite lithologies. The phyllite has not been imported into Petrel as it has been assumed that it represents the basal unit to the active groundwater flow system. Whilst this is a reasonable assumption for the purposes of determining the primary groundwater flow pathways, variations in hydraulic properties within the phyllite will be required to evaluate the hydraulic controls on pit slope depressurisation.

[33]Petrel, développé par Schlumberger

Pic de Fon Northern Zone

- Figure I 1A: The geological section at the rear of the Petrel image (northing 944890), is at a similar northing to the Whisky 1 springs. The groundwater level here, at 1070 mRL ('**a**') is the same elevation as the phyllite shear on the east of the orebody which is at a low elevation point on this northing line ('**b**'). Groundwater is flowing over the phyllite into the Whisky 1 valley headwater area. Moving south, the phyllite shear increases in its elevation and supports higher groundwater levels to its west within the orebody ('**c**'). Groundwater levels are lower in a central trough of mineralisation at an elevation controlled by an overspill further south, at around 1340 mRL–1345 mRL (see Figure F-1 B arrow 'a').
- Figure I 1B: Moving south the groundwater level in the deepest trough of mineralisation is controlled by overspill of the IPC at around 1340 mRL ('**a**') west into the deep IPF/IRF orebody to the west of the ridgeline. Water levels in the eastern orebody trough are assumed to be flat at the elevation of this overspill ('**b**'). It is likely that groundwater over-spilling west, ponds within the friable itabirite ('**c**') to then drains slowly through the adjacent IPC via the fracture network into the Western Spur valley. Groundwater flow to the east is restricted by the phyllite shear.
- Figure I 2A: The groundwater level is within the itabirite at Pic de Fon, with high groundwater levels supported by the low permeability phyllite shear to the east ('***a***'). Groundwater flow is from Pic de Fon into the Western Spur where the groundwater level is at around 1235 mRL ('***b***'). The mechanism by which groundwater flows from the Western Spur orebody into the Western Spur valley appears to be structurally controlled as compact itabirite surrounds the mineralisation at the 1235 mRL level. The relatively shallow hydraulic gradient between the groundwater in the Western Spur orebody and the springline in the valley suggests that a highly transmissive fissure exists through which groundwater can discharge from the Western Spur orebody. This fissure may be associated with a structure that appears to control the spring line on the western side of the valley.
- Figure I 2B: To the east of Pic de Fon and the phyllite shear, groundwater levels are much lower, measured as 1327 mRL in PDF322 compared to over 1400 mRL on Pic de Fon ('**a**'). The groundwater level within the itabirite is high adjacent to Pic de Fon, controlled by the upwelling phyllite ('***b***'). Moving south the shallow mineralisation deepens ('***c***') and allows groundwater flow southwards, so that the groundwater is at an elevation of around 1185 mRL in a trough of mineralisation east of the shear ('***d***'). To the west of the phyllite shear in the Elephant Rock area, the groundwater surface is relatively flat at 1342 mRL–1350 mRL, with a gradient directing flow to discharge into the Whisky 2 catchment.

Pic de Fon Central Zone

- Figure I 3A: Further south, in the central zone, groundwater levels in the phyllite east of the orebody remain very high compared to the orebody (1290 mRL measured in PDF434) indicating very low permeability within the phyllite ('***a***'). Within the orebody the groundwater level data indicate a relatively flat water table at around 1080 mRL ('***b***').
- Figure I 3B: The groundwater level does not obviously decrease in elevation to the south; however, higher groundwater levels ('***c***') are measured closer to the phyllite shear ('***a)***' in the east, where the IPC boundary shallows. The groundwater level in the western portion of the ore body remains at around 1080 mRL ('***b***')

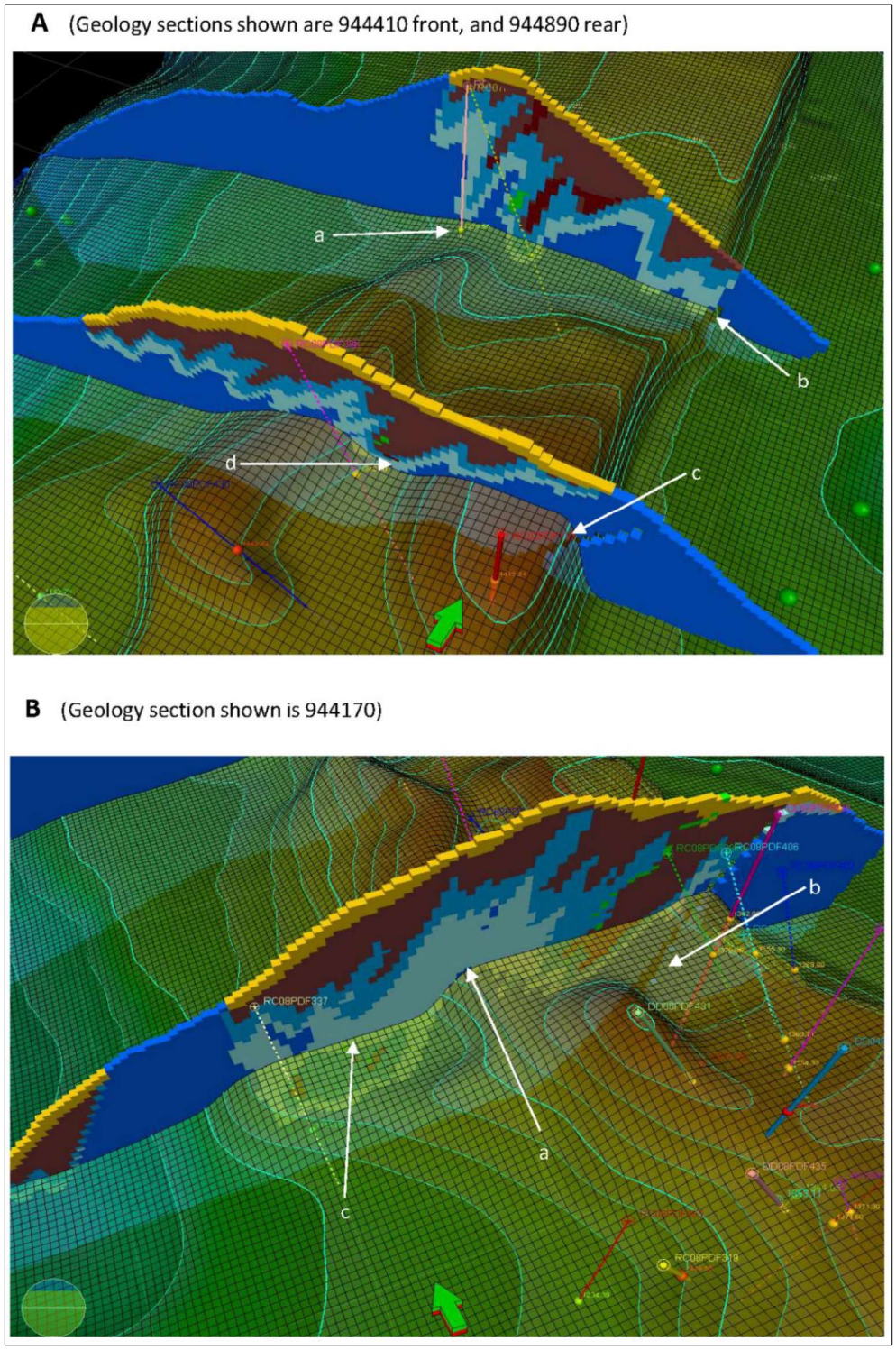

Figure I 14: Petrel model screenshots of northern Pic de Fon (from SWS, 2012)

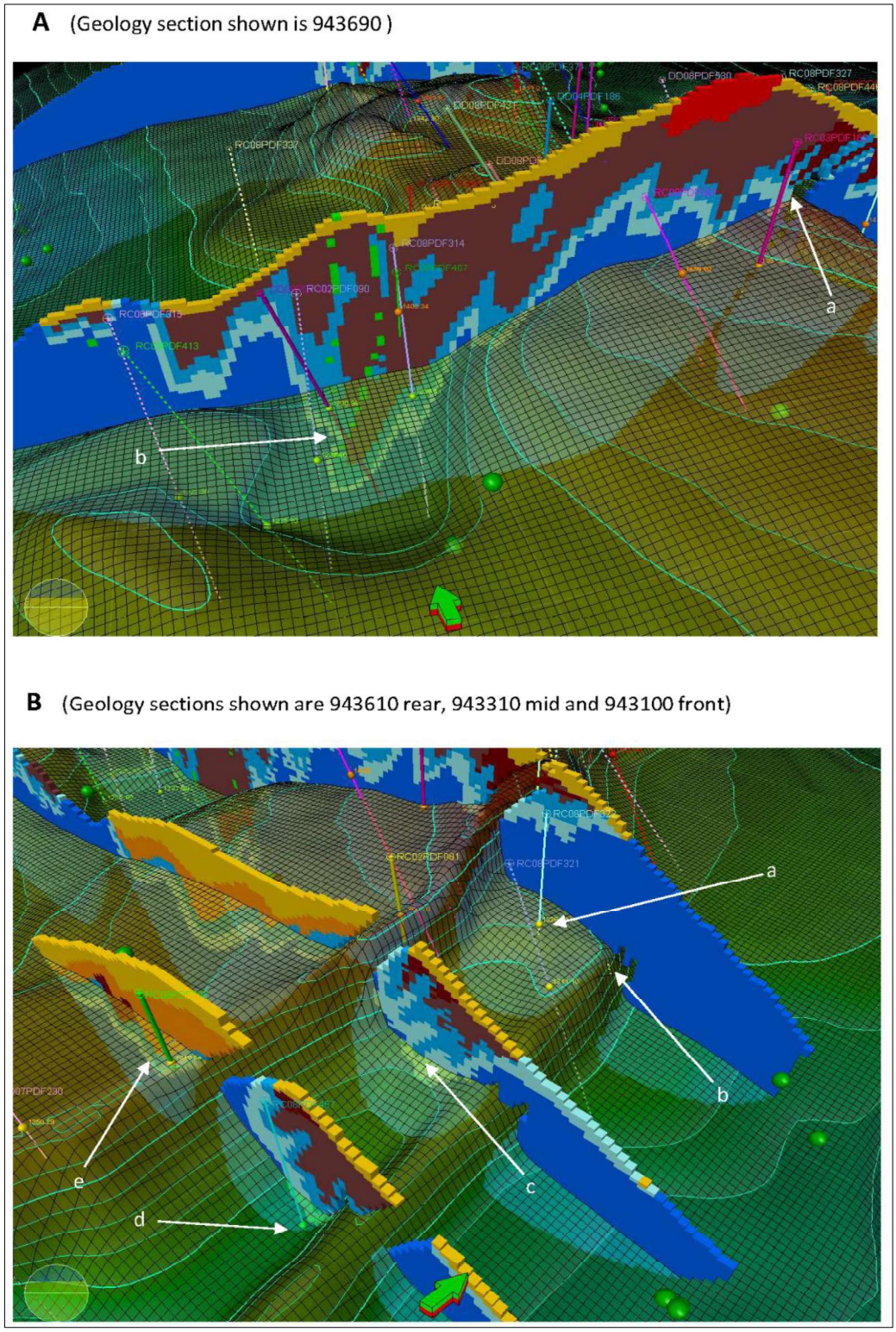

Figure I 2: Petrel model screenshots of northern Pic de Fon (Pic de Fon into Western Spur) (from SWS, 2012)

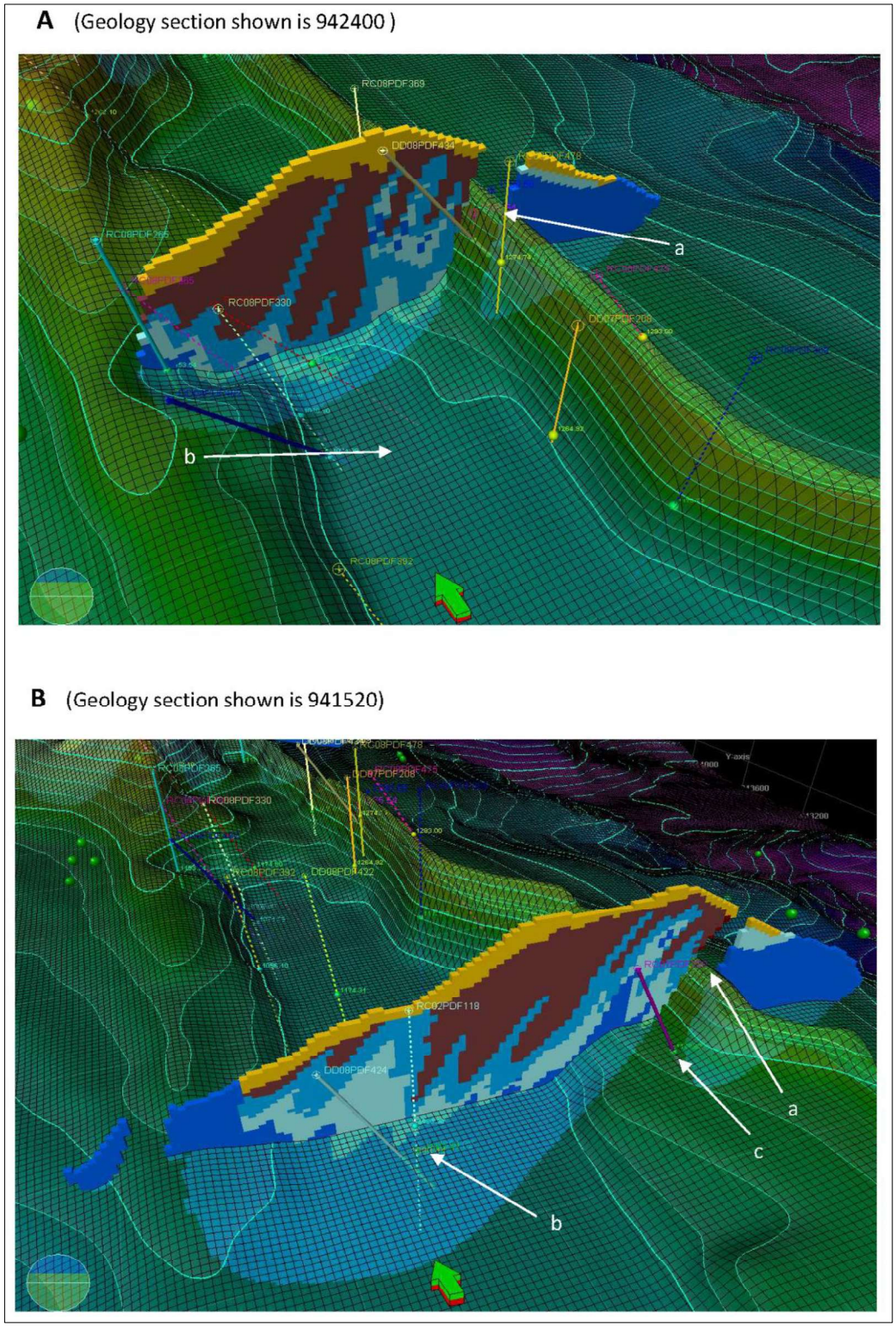

Figure I 3: Petrel model screenshots of central Pic de Fon (from SWS, 2012)